ELSEVIER

Journal of Power Sources 92 (2001) 26–34

JOURNAL OF POWER SOURCES

www.elsevier.com/locate/jpowsour

Thermodynamic model and parametric analysis of a tubular SOFC module

Stefano Campanari Ph.D.*

Department of Energetics, Polytechnic of Milan, Piazza Leonardo da Vinci 32, 20133 Milan, Italy

Received 15 February 2000; received in revised form 26 April 2000; accepted 2 May 2000

Abstract

Solid oxide fuel cells (SOFCs) have been considered in the last years as one of the most promising technologies for very high-efficiency electric energy generation from natural gas, both with simple fuel cell plants and with integrated gas turbine-fuel cell systems. Among the SOFC technologies, tubular SOFC stacks with internal reforming have emerged as one of the most mature technology, with a serious potential for a future commercialization. In this paper, a thermodynamic model of a tubular SOFC stack, with natural gas feeding, internal reforming of hydrocarbons and internal air preheating is proposed. In the first section of the paper, the model is discussed in detail, analyzing its calculating equations and tracing its logical steps; the model is then calibrated on the available data for a recently demonstrated tubular SOFC prototype plant. In the second section of the paper, it is carried out a detailed parametric analysis of the stack working conditions, as a function of the main operating parameters. The discussion of the results of the thermodynamic and parametric analysis yields interesting considerations about partial load SOFC operation and load regulation, and about system design and integration with gas turbine cycles.

Keywords: SOFC model; Thermodynamic analysis; Parametric analysis

1. Introduction

The quest for higher efficiencies in electric power generation from fossil fuels has always pushed the research on fuel cells, and many new technologies have been tested in the last years in the field of high temperature fuel cells. Solid oxide fuel cells (SOFCs) are particularly promising for their high operating temperature that makes them suitable for integration with gas turbine cycles and cogeneration [1–3]. The tubular SOFC technology, mainly developed by Siemens–Westinghouse [4], has led to the most advanced SOFC demonstration plant, installed in The Netherlands with a 100 kW capacity, and to various demonstration projects in the size 300 kW–2 MW to be started within the current year. Other SOFC technologies (planar, monolithic) frequently analyzed in literature have been developed up to a smaller scale, and are still in a much earlier development stage. This paper focuses on a thermodynamic model of a tubular SOFC stack, dealing with the analysis of the effects of a variation in the operating conditions on the stack performances.

2. The SOFC model

The model applies to a tubular SOFC stack fed with natural gas with internal reforming, schematically shown in Fig. 2. The model calculates:

1. The thermodynamic properties and chemical composition of anode and cathode outlet and stack exhaust gases.
2. The SOFC thermal balance (efficiency, heat generated).
3. The SOFC second law analysis (entropy losses), as a function of U_f, U_a (fuel and air utilization), of the inlet compositions and average working temperature.

The model also calculates a number of data concerning stack internal flow compositions and thermodynamic conditions (prereformed and reformed fuel, depleted fuel and air flow) and SOFC operating parameters. Calculation is divided in a step sequence and discussed as following.

2.1. Calculation of the requested fuel flow

The model first calculates the number of moles of hydrogen (generated by the fuel gas) consumed in a single passage inside the fuel cell, without fuel recirculations. It is then

* Fax: +39-2-23993940.
E-mail address: stefano.campanari@polimi.it (S. Campanari).

0378-7753/01/$ – see front matter
PII: S0378-7753(00)00494-8

Nomenclature

A_c	cell active area (cm^2)
e^-_{charge}	electron charge 1.602×10^{-19} C
F	Faraday's constant (96439 C/mol, Eq. (9))
i_c	cell current density (A/cm^2)
K_{eq}	CO-shift-reaction equilibrium constant
m_X	mass flow of the chemical specie X (mol/s)
N_{av}	Avogadro's number (6.022×10^{23})
p	pressure (bar)
S/C	steam-to-carbon ratio
T	temperature (K or °C)
U_a	air utilization factor (Eq. (12))
U_f	fuel utilization factor (Eq. (11))
V_c	cell voltage (Eq. (8))
W_{rev}	reversible work (J/kg)
W_{el}	electric work (J/kg)
X_{CH_4}	methane contribute to hydrogen formation
X_{CO}	carbon monoxide contribute to hydrogen formation
ΔS	entropy loss (J/kg K)
ΔT_{co}	operating/exhaust temperature difference at cell outlet
ΔV	voltage difference (Eqs. (4)–(7))
η_{el}	electrical efficiency (Eq. (9))
Γ_{H_2}	fuel equivalent hydrogen content (Eq. (10))

Subscripts

amb	ambient
op	operation
f	fuel
ref	reference conditions
cons	consumed

Acronyms

AES	air electrode supported
LHV	fuel lower heating value (J/mol)
SOFC	solid oxide fuel cell

calculated the pseudo-stoichiometric air/fuel ratio (R_f), which is equal to the number of moles of air requested to oxidize 1 mol of fuel with the given U_f and U_a ratios.

The fresh air flow is known as an input data, and the requested fuel flow is then calculated by

$$m_{fuel,requested} = \frac{m_{air,inlet}}{R_f} \quad (1)$$

2.2. Calculation of internal reforming

The hydrocarbons are converted into a H_2–CO–CO_2–H_2O mixture by steam reforming, exploiting steam contained in the partially recirculated anode exhaust gases. The recirculated fraction is calculated to obtain a given steam/carbon (S/C) ratio, defined as the ratio between the number of the H_2O molecules and the number of the C-atoms of combustible components [5].

Two separated steps calculate mixing and prereforming on the fuel side:

1. Calculation of the mixing of inlet fuel (at a given temperature) with a recirculated fraction of the anode exhausts with an enthalpy balance. The anode and cathode exhaust temperatures are set to $T_{op}-\Delta T_{co}$, where ΔT_{co} is assigned as input value (Table 1).
2. Calculation of the prereforming of mixed fuel as an adiabatic (constant enthalpy) process, reaching thermodynamic equilibrium. The program calculates the prereformed fraction of hydrocarbons (HC) as the ratio $HC_{moles,reformed}/HC_{moles,inlet}$.

Fuel recirculation is sustained by fresh-fuel-driven ejectors; the model calculates the requested inlet fuel pressure based on momentum and mass balances with a nozzle isentropic efficiency of 0.92.

Fuel is then completely reformed inside the fuel cell, according to the steam-reforming and CO-shift reactions

$$C_nH_m + (\tfrac{1}{2}m - 1)H_2O \rightarrow (m-1)H_2 + nCO \quad (2a)$$

$$CO + H_2O \rightarrow H_2 + CO_2 \quad (2b)$$

where it is considered that the reforming reactions are completely developed, thanks to the very high temperature conditions and to the catalytic effect of the anode materials. The CO-shift reaction is considered to reach thermodynamic equilibrium, with an equilibrium constant given by

$$K_{eq} = \frac{[H_2]\times[CO_2]}{[CO]\times[H_2O]} \quad (3)$$

(molar concentrations in square columns) calculated for the selected cell outlet temperature.[1]

The outlet fuel composition is calculated iteratively to satisfy the requested U_f and the calculated K_{eq}. The calculation is performed by applying the conservation equations for the carbon and hydrogen moles number; it is supposed for simplicity that CO is not oxidized directly but only by the shift reaction. The model finally calculates two global values of U_a and U_f, accounting for the fuel recirculation effects.

2.3. Cell voltage and efficiency

Calculation of cell voltage is performed as a function of the current density, of the operating temperature, of the operating pressure (simple average value of inlet and outlet pressures) and of the reactant and products composition.

The primary influence of current density (i_c) on the SOFC performance (by ohmic, activation and concentration losses) is expressed by the reference correlation for $V_0(i)$ shown in

[1] The value of K_{eq} is not influenced by pressure because the moles number is constant across the shift reaction.

Table 1
Assumptions and operating parameters for the basic FC configuration of Fig. 2

$\Delta p/p$ air/fuel side	5%/2%
$\Delta p/p$ auxiliary combustion	3%
SOFC thermal losses (radiation, external convection)	2%
Auxiliary combustion efficiency	99.5%
dc–ac and power conditioner efficiency	92%
Fuel utilization factor, U_f at input (single passage)	69%
Fuel utilization, U_f (global, with recirculation)	85%
Air utilization factor, U_a (global)	17.9%
Cell operating temperature, T_{op}	1000°C
Temperature difference between T_{op} and cell exhausts, ΔT_{co}	90°C
Current density, i_c	180 mA/cm^2
S/C and O/C ratio (global)	1.8/2.04
Calculated cell voltage, V_c	0.69 V
Calculated ejector fresh fuel pressure ratio, p_{fuel}/p_{cell}	≈3.0
Calculated hydrocarbon fraction prereformed	17%
Fuel composition: CH_4 81.3%–C_2H_6 2.9%–C_3H_8+C_4H_{10} 0.6%–CO_2 0.9%–N_2 14.3%	

Fig. 1. The $V_0(i)$ curve is obtained by interpolation of experimental data [6,8] at standard operating conditions (fuel composition: 67% H_2–22% CO–11% H_2O, U_f=85%, U_a=25%, T=1000°C, p=1 bar). Calculation of the actual cell voltage value, V_c, is then performed by semiempirical correlation [6,7] accounting for the differences due to the real operating conditions.

These correlation are expressed by the logarithmic corrections of Eqs. (4)–(7); they are derived by the Nernst potential equation, and modified with the adoption of an empirical multiplying coefficient.

2.3.1. Operating pressure effect

$$\Delta V_p(\mathrm{mV}) = C_1 \log\left(\frac{p}{p_{\mathrm{ref}}}\right) \tag{4}$$

for operating pressures in the range 1–10 bar, where the theoretical Nernst constant C_1 would be 59 mV per decade; for tubular AES cells a greater value is assumed [8], equal to 76 mV per decade.

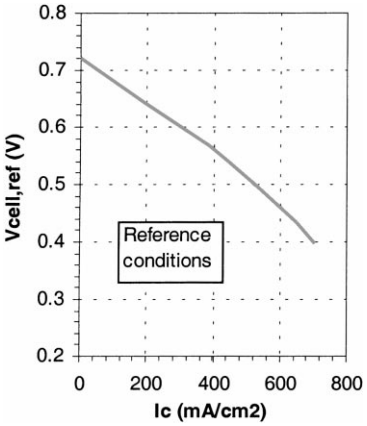

Fig. 1. Cell voltage at reference operating conditions (see text).

2.3.2. Operating temperature

$$\Delta V_T(\mathrm{mV}) = K_T(T - T_{\mathrm{ref}}) \times i_c \tag{5}$$

where the constant K_T =0.008 for temperatures in the range 900–1050°C.

2.3.3. Cathodic flow (oxidizer) composition

The use of pure oxygen instead of air as oxidizer, or the variation of U_a, changes the oxygen partial pressure at cathode and, thus, the cell reversible Nernst potential E_{rev} and the cell concentration polarization. The corresponding cell voltage correction is

$$\Delta V_{\mathrm{cat}}(\mathrm{mV}) = 92 \log\left[\frac{P_{O_2}}{(P_{O_2})_{\mathrm{ref}}}\right] \tag{6}$$

where p_{O_2} is the average oxygen partial pressure in the cathode flow (within the range 0.16–0.20).

2.3.4. Anodic flow (fuel) composition

The fuel flow composition influences the cell voltage. Higher voltage values are generated with fuels with a higher hydrogen fraction. It is possible to evaluate the effect of a variation in the fuel flow composition through the ratio of hydrogen and steam partial pressures.

$$\Delta V_{\mathrm{an}}(\mathrm{mV}) = 172 \log \frac{p_{H_2}/p_{H_2O}}{(p_{H_2}/p_{H_2O})_{\mathrm{ref}}} \tag{7}$$

for partial pressure ratios in the range 0.9–6.9, T_{op}=1273 K and air as oxidizer (the theoretical Nernst variation would be 126 mV per decade).

The flow compositions in the expression of ΔV_{cat} and ΔV_{an} are calculated, for co-flow configurations like tubular SOFCs, at the fuel cell outlet. For this reason, these corrections are influenced also by the U_f and U_a values. The sum of these corrections gives

$$V_c = V_{\mathrm{ref}} + \Delta V_p + \Delta V_T + \Delta V_{\mathrm{cat}} + \Delta V_{\mathrm{an}} \tag{8}$$

The cell electrical efficiency $W_{el}/LHV_{fuel,in}$ is then a function of the cell voltage, of the fuel utilization factor and of the inlet fuel composition [9], according to

$$\eta_{el} = \frac{W_{el}}{LHV} = \frac{nFE}{LHV} = \frac{nFV_c \times U_f \times \Gamma_{H_2}}{LHV} \quad (9)$$

The quantity Γ_{H_2} is the fuel equivalent hydrogen content, expressed for a fuel mixture of H_2–CH_4–CO–H_2O by the following equation:

$$\Gamma_{H_2} = X_{H_2} + X_{CH_4} + X_{CO} \quad (10)$$

X_{CH_4} and X_{CO} are the methane and carbon monoxide contributes to hydrogen formation, accounting for a complete hydrocarbon reforming and for the additional contribute of the CO-shift reaction.

The fuel utilization factor is then defined as

$$U_f = \frac{m_{H_{2,consumed}}}{m_{H_{2,in}}} = \frac{m_{H_{2,consumed}}}{m_{H_{2,in}} + m_{CO_{in}} + 4 \times m_{CH_{4,in}}} \quad (11)$$

where 4 mol of H_2 (three by steam reforming, one by the shifted CO) are generated by each CH_4 mole.

Similar contributes would arise by the reforming of other hydrocarbons.

On the oxidizer side, an air utilization factor is defined as follows:

$$U_a = \frac{m_{O_{2,in}} - m_{O_{2,out}}}{m_{O_{2,in}}} = \frac{m_{O_{2,consumed}}}{m_{O_{2,in}}} \quad (12)$$

The air utilization factor is proportional to the oxygen quantity extracted from the air flow to oxidize the fuel. For a cell of assigned size and active surface area, and with an assigned inlet air flow (coming for example, from a compressor), any variation of U_a is generated by a proportional variation of the number of oxygen ions conducted by the electrolyte. This number is then proportional to a variation of the cell current density and overall current output.

The following equation shows this relationship, where the oxygen flow m_{O_2} is expressed in kg/s and the mole number (n_{O_2}) and ion number (n_{i_O}) are intended as units per second

$$m_{O_{2,cons}} = \frac{32}{100} \times n_{O_{2,cons}} = \frac{0.032}{2 \times N_{AV}} \times n_{i_{O_{cons}}} = \frac{0.032 i_c \times A_{cell}}{4 \times N_{AV} \times e^-_{charge}} = \frac{0.032 i_c A_{cell}}{4F} \quad (13)$$

This consideration is particularly important for partial-load and transient operation of the fuel cell, where an air by-pass system can be used to avoid excessive variations of U_a in response to fluctuations in the power demand and in the cell current output.

2.4. Heat generation and exhaust gas temperature

The heat generated by irreversibility at the electrodes structure is given to the fuel and air flow, and partially lost by the stack external canister. A significant fraction of the heat is used by the endothermic reforming reactions, thus, reducing the requested cooling air flow and enhancing the fuel heating value.

A thermal balance across the whole cell calculates the fraction of heat (Q_{air}) given to the air flow and partially lost to the external atmosphere

$$Q_{air} = m_{fuel,in} \times H_{fuel,in} - m_{fuel,out} \times H_{fuel,out} - W_{el} \quad (14)$$

where H is comprehensive of the enthalpy of formation and, thus, of chemical energy. This balance includes also the fuel mixing and reforming processes.

The SOFC stack finally generates a single outlet stream: cathode and anode exhausts (spent air and spent fuel) react burning in a combustion plenum. The generated exhaust gas then preheats the inlet air flow. The requested air temperature (T_0) after preheating is known from the previous calculation of the SOFC heat generation. With another calculation option [10], it is possible to automatically set the SOFC operating condition (with different U_a and U_f values) in order to match a given air inlet temperature. Finally, the calculation of the exhaust pressure is done with given values of pressure losses.

2.5. Aim of the model

The proposed SOFC model has been developed with the aim of enabling a detailed thermodynamic and parametric analysis of the SOFC operation, with the further perspective of being integrated in an existing gas–steam cycle simulation code for the analysis of combined gas turbine–SOFC cycle performances [3]. Some of the model core assumptions, as the semiempirical cell voltage calculation, deliberately avoid a detailed analysis of the cell physical structure and the consequent introduction of a number of cell microscopic and geometrical parameters (components thickness, porosity, ohmic resistivity, etc.). This simplified approach makes the model particularly suitable of being easily calibrated, following the continuous and rapid technological development in the field of SOFC materials [8] and design [4].

3. Calibration of the SOFC model and thermodynamic analysis

The SOFC model discussed in this paper has been calibrated on the performances of a 100 kW prototype plant, which has been working at atmospheric pressure and about 48% LHV electrical efficiency, running on natural gas. Details about these plant characteristics have been found in recent literature [2,11,12]. Based on the available information, the atmospheric SOFC stack basic configuration shown in Fig. 2 has been set, with the assumptions listed in Table 1.

The inlet air temperature has been set to 630°C, and the inlet fuel temperature to 200°C; a fuel utilization factor of

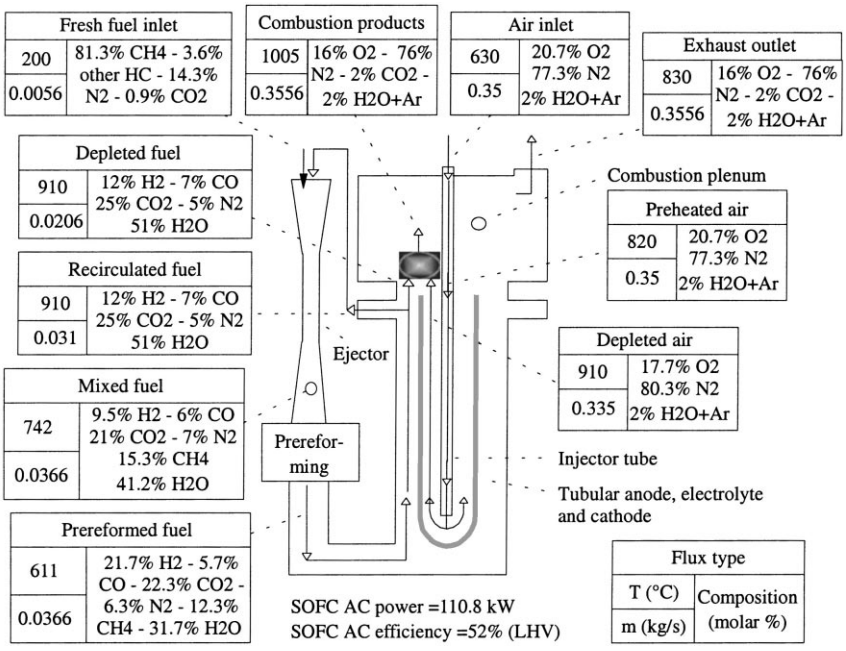

Fig. 2. Tubular SOFC stack; operating conditions calculated with the assumptions of Table 1.

0.69 for a single passage leads to a global U_f of 85%. The remaining fuel is burnt with depleted air in the combustion plenum, generating hot gases, which are used to preheat the inlet air flow before being exhausted.

In this paper, the focus is set on the simple SOFC stack, not considering auxiliary equipment losses (inlet air blower, fuel desulphurizer) and external components (recuperative air preheater).

The calculated stack LHV efficiency of 52% should, therefore, be lowered for any external or auxiliary electric consumption: adopting a 7 kW blower and fuel compressor system, the total electric LHV efficiency becomes 48.5%. Together with the calculated flow compositions and temperatures, these figures show good agreement with the available experimental result [2]. Tables 2 and 3 summarizes the first (I) and second (II) law analysis for this stack.

In Table 3 the II law or reversible work losses of the SOFC module in Fig. 2 are listed, defined as follows:

$$\Delta\eta_{II} = \frac{T_{amb}\Delta S}{W_{rev,f}} \quad (15)$$

The very high II law efficiency (over 86%) achieved by the SOFC system is of course its most promising feature. It is possible to notice how this value could be improved by: (i) lowering the dc–ac conversion losses: higher efficiencies could probably be achieved with larger scale system; (ii) lowering the electrochemical losses, i.e. getting higher cell voltages and lower electric and ionic resistance with improved cell design and material development [4]. The operation at higher fuel utilization could further improve the cell efficiency and reduce the auxiliary combustion losses.

The analysis of Tables 2 and 3 clearly shows that a large enthalpy and reversible work flow is associated both with the preheated inlet air (51.5 and 33%, respectively) and with the hot exhaust gases (72.6 and 52.4%). It is then of particular importance to design an efficient heat-recovery and air preheating system around the SOFC stack. This consideration would become fundamental if the SOFC stack should be operated at higher pressure and fed with a more energy-demanding compressed and preheated air flow, as in integrated gas turbine–SOFC hybrid cycles [3].

Table 2
First law analysis for the SOFC module of Fig. 2

	% on total inlet	Q_{th} (kW)
Enthalpy flows		
Fuel inlet	48.5	214.8
Preheated and compressed inlet air flow	51.5	228
Depleted outlet fuel flow	–	70.3
Internal air preheating	–	76.5
Cell electrode air heating	–	23.6
Heat losses		
Auxiliary combustion	0.07	0.3
dc–ac and power conditioner efficiency	2.18	9.7
Thermal losses	0.11	0.5
Total losses	2.36	10.5
Enthalpy flow associated with exhaust gases	72.6	321.5
Net electric power production	25.04	110.8
Total	100	–
Electric efficiency [W_{el}/LHV$_{fuel,in}$]	52	–

Table 3
Entropy losses for the SOFC module of Fig. 2[a]

	% on total inlet	$\Delta\eta_{II}$ (Eq. (15))
Reversible work associated with inlet flows		
Inlet fuel	66.6	–
Preheated and compressed inlet air	33.4	–
Reversible work losses		
Electrochemical process and heat exchange at electrodes	2.73	4.10
Auxiliary combustion	4.62	6.94
dc–ac and power conditioner efficiency	2.93	4.40
Anodic recirculation and mixing	1.20	1.80
Air preheating	1.09	1.64
Pressure losses	1.03	1.55
Thermal losses	0.25	0.37
Total losses	13.85	20.80
Reversible work associated with exhaust gases	52.4	–
Net electric work	33.7	–
Total	100	–
II law efficiency $[\Sigma(W_{rev,out})/\Sigma(W_{rev,in})]$	86.1	–

[a] Numbers in the last column are reversible work losses divided by the inlet reversible work associated with the fuel flow only.

4. Parametric analysis

Starting from the 'nominal' conditions listed in Table 1 and shown in Fig. 2, it is possible to discuss the effects of a variation of each of the most interesting SOFC operating parameters. A variation of four operating parameters (i_c, U_f, U_a, S/C ratio) of the SOFC module has been considered, and a detailed analysis of their mutual dependencies and their effects on the cell efficiency, power output and other cell working conditions has been carried out. The obtained results are summarized in detail by Table 4, and qualitatively discussed in the following.

It should be preliminarily noticed that when the cell operating conditions become substantially different from the nominal conditions, some parameters could trespass into areas of practical unfeasibility (for example with too low cell inlet temperatures or S/C ratios, too high utilization factors or preheating temperatures).

4.1. Variation of i_c and U_a

With an increase of i_c from 100 up to 400 mA/cm^2, the cell voltage and efficiency decreases and the cell specific electric power (kW generated/inlet fuel flow) becomes lower; the total power production conversely increases. The fuel chemical energy not converted into electricity is transformed into heat released to the reactant flows, and mainly to the air flow; by this way the air preheating duty decreases and the module exhaust temperature T_{exh} rises.

As already shown by Eq. (13), it is possible to change i_c with constant U_a only with a different air flow (obtained by a regulation of the compressor airflow or by an air by-pass system) or with a different cell active area.[2] The combined variation of i_c and U_a, together with the consequent variation of the inlet fuel mass flow, is the main way to regulate the stack electric power production.

The first four rows in Table 3 are calculated with the SOFC stack operating at constant air flow (0.35 kg/s), and with the air utilization factor changed proportionally to the requested cell current density (case labeled A). The second four rows are calculated with the SOFC stack operating at constant air utilization factor U_a, and with the air flow adjusted proportionally to the requested current density (case labeled B).

By increasing the cell current density, the oxidized fuel flow increases. A consequently larger exhaust fuel flow is burned in case A with the same air flow, and in case B with a proportionally larger air flow, thus, giving respectively an increased or constant combustion temperature, T_{comb}.

Case A shows a sharper decrease of the cell voltage, due to the combined effects of a higher current and a lower oxygen concentration. The consequent lower cell efficiency and larger heat generation increases the internal air flow temperature rise. Thus, the air preheating duty decreases rapidly, and by the combined effect of a higher combustion temperature (T_{comb}) the stack generates much hotter exhaust gases. In case B the cell voltage decay is smoother, and the air preheating duty shows a more limited decrease. As the combustion temperature is almost constant, the stack exhaust temperature increases slowly.

The electric power generated in the two cases is almost identical, except for small differences due to limited variations of the cell voltage, because the amount of consumed oxygen ($m_{air} \times U_a$) is practically constant.

The overall SOFC module behavior is expressed by Fig. 3. The effective regulation of the cell load can be obtained for any requested cell current by changing both the air utilization factor and the air mass flow, moving between the couples of lines shown in Fig. 3.

The operation at low cell current density yields a high electrical efficiency but decreases the stack power production and the stack exhaust temperature. These two effects are both undesirables for a practical power plant application, where the lowest capital costs are required and the SOFC is likely to be integrated with gas turbine cycles.

As shown by case A, an increase of the cell air utilization factor leads to a higher power generation (higher electric power production per kg/s of inlet air) and to a large increase of the SOFC stack exhaust temperature. The combination of these two effects is beneficial for power plant applications where an increase of the plant specific work is requested.

[2] This possibility involves a preliminary project choice dedicated to the individuation of the appropriate cell number, or the adoption of an apposite regulation system capable of bypassing some cells and making them inactive in hot-stand-by conditions.

Table 4
Parametric analysis of the SOFC module operating conditions and efficiency with a variation of i_c (mA/cm^2), U_a, U_f and S/C ratio[a]

	Changed parameters		T_{comb} (°C)	S/C	m_{rec} (kg/s)	U_a (%)	$U_{f,\ global}$ (%)	V_c (mV)	ΔT_{preh} (°C)	T_{exh} (°C)	%mol O_2	$Q_{th,fuel,in}$ (kW)	W_{el} (kW)	η_{el}%
	i_c	m_{air}												
Variation of i_c (A)	100	0.35	963.8	1.8	0.049	9.92	85	732	239.4	734	19.1	120.2	65	55.1
(m_{air} constant)	200		1014.5		0.098	19.8		683	176.0	852.8	17.3	233.4	121.3	51.5
	300		1062		0.146	29.7		639	92.7	980.5	15.5	353.7	169.9	48.1
	400[b]		1107		0.195	39.7		594	15.0[b]	1094	13.6	474	210.9	44.7
Variation of i_c (B)	100	0.19	1004.7	1.8	0.088	17.9	85	729	205.5	813.8	17.7	120.2	64.6	54.9
(m_{air} constant)	200	0.39						684	186.8	831.7		233.4	121.6	51.5
	300	0.58						644	170	847.5		353.7	171.6	48.5
	400	0.78						604	153.3	863.3		474	214.8	45.5
Variation of U_f single		0.6	1043.1	1.62	0.097	17.9	80	720	213.5	846.1	17.7	226.4	115.4	51.1
passage (i_c, U_a,		0.7	1000.7	1.82	0.087		85.5	689	188.1	826.3		211.0	110.2	52.3
m_{air} constant)		0.75	982.5	1.93	0.083		88.1	671	175	820		205.1	107.4	52.5
		0.8	965.7	2.03	0.080		90.6	651	161	816		198.1	104.4	52.3
		0.85	950.0	2.13	0.076		93.1	625	146.1	814		191.0	100.0	51.6
		0.9	935.6	2.24	0.073		95.4	591	127.5	816.8		183.9	94.6	50.1
Variation of S/C (i_c, U_a,		1.4	1011.8	as input	0.066	17.9	84.0	698	195.0	831.2	17.7	214.9	111.9	52.1
m_{air} constant)		1.6	1008.2		0.076		84.5	696	192.7	829.6		213.7	111.4	52.1
		1.8	1004.7		0.088		85.0	693	190.5	828.1		212.2	110.8	52.2
		2.0	999.1		0.097		85.8	688	186.4	826.2		210.9	110.3	52.3
		2.2	996.5		0.109		86.1	685	185.1	824.8		209.7	109.7	52.3
		2.5	994.1		0.129		86.4	683	183.8	823.4		208.2	109	52.4

[a] Unchanged parameters have the nominal values listed in Table 1. Inlet fuel and air temperature are kept constant (200 and 630°C, respectively).
[b] In this case the inlet air temperature is $T_{air} = 600$°C.

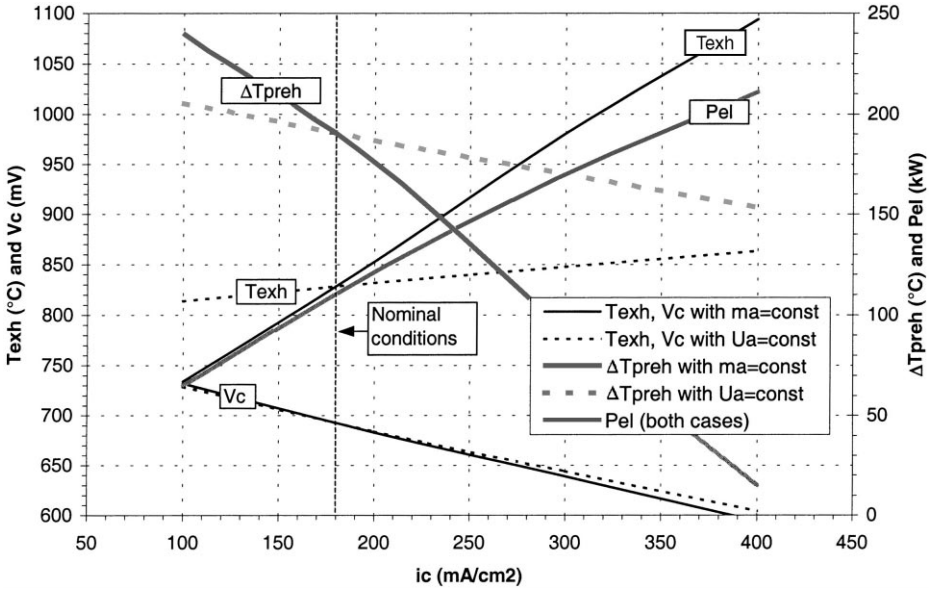

Fig. 3. Effects of a variation of the cell current density on the stack exhaust temperature (T_{exh}), cell voltage (V_c), air preheater duty (ΔT_{preh}) and stack electric power (P_{el}).

4.2. Variation of U_f

A variation of U_f from 0.6 to 0.9 on a single passage leads to a corresponding increase of U_f global, including recirculation effects, from 0.80 up to 0.95. This variation can be operatively obtained by limiting the cell fuel input, as the fuel flow requested to exploit the available oxygen (with constant air flow, i_c and U_a) diminishes at increased U_f.

Even holding the anode recirculation ratio unchanged the global S/C ratio increases, because the recirculated gases are richer in steam and poorer in CO (transformed into CO_2 by the shift reaction). The recirculated fuel flow decreases more than proportionally to the inlet fuel flow, thanks to its higher steam fraction. The requested fuel pressure at the ejector decreases.

A higher U_f also leads to a lower depleted fuel heating value and, thus, to a lower auxiliary combustion temperature (T_{comb}). The cell voltage decreases, due to the reduced fuel minimum hydrogen content and higher anode polarization losses. The cell generates more heat, released to the reactant flows, and the air preheating duty decreases. The lower combustion temperature leads anyway to a decrease of the stack exhaust gas temperature.

The electric efficiency, which is proportional to $V_c \times U_f$, rises with U_f in spite of the slightly lower cell voltage, reaching a maximum for a value of U_f close to 0.88. Only for higher fuel utilization the efficiency decreases due to the growing effects of the voltage decay for concentration losses. These results are shown in Fig. 4. It is possible to notice also that the electric power output decreases, even if supported by the higher electric efficiency, because a lower fuel flow (with lower thermal power input) is progressively used.

4.3. Variation of the S/C ratio

If the steam-to-carbon ratio is increased from S/C=1.4 up to 2.5 (with constant U_a, i_c, air and fuel flow) the corresponding global fuel utilization factor $U_{f,\,global}$ increases due to the higher mass flow of fuel recirculated and consumed. As the air flow (m_{air}) and the air utilization factor (U_a) are constant, then the amount of consumed oxygen is also constant. Thus, the fuel mass flow shall be slightly decreased to accommodate the larger U_f.

The cell voltage decreases together with the electric power production (Fig. 5), while the module efficiency Eq. (9) slightly increases.

The auxiliary combustion temperature decreases due to the lower depleted fuel heating value, while the increased

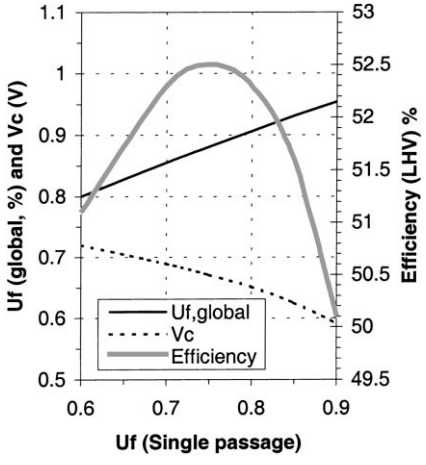

Fig. 4. Effects of a variation of U_f on a single passage over the global U_f and the cell voltage and efficiency (m_{air} constant, m_{fuel} decreased).

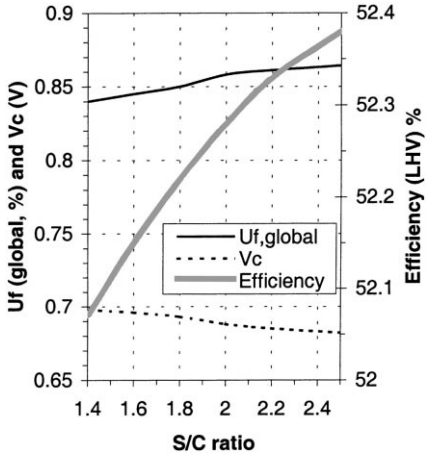

Fig. 5. Effects of a variation of the S/C ratio over the global U_f and the cell voltage and efficiency (m_{air} constant, m_{fuel} decreased).

cell heat generation reduces the air preheating duty; the combination of the two effects leads to almost constant SOFC stack exhaust temperatures.

The increase of S/C yields also an increase of the mass flow ratio between fresh fuel and recirculated fuel, leading to the requirement of a higher fresh fuel pressure to sustain the ejector recirculation. It would be generally desirable to operate with the lowest S/C ratio, compatibly with the problem of carbon deposition, to have the possibility of reducing the fresh fuel pressure.

5. Conclusions

A thermodynamic model for a tubular SOFC stack fed with natural gas with internal reforming, exhaust gas residual combustion and internal air preheating has been developed. The model has been calibrated over the performances of a recent prototype plant, showing the capacity of predicting accurately the SOFC operating conditions. A thermodynamic analysis of the SOFC stack losses has been carried out according to the first and second law, showing the importance of an efficient design of the heat-recovery and air preheating systems around the SOFC stack. The parametric analysis of the stack behavior, based on a variation of the cell operating parameters, yields a detailed insight on the influence of each variable on the cell efficiency and electric power output and on load regulation techniques.

References

[1] S.P. Harvey, H.J. Richter, Gas turbine cycles with solid oxide fuel cells — Part I and II, J. Energy Resour. Technol. 116 (1994).
[2] S. Veyo, W. Lundberg, Solid oxide fuel cell power system cycles, ASME paper 99-GT-356, International Gas Turbine and Aeroengine Congress and Exhibition, Indianapolis, June 1999.
[3] S. Campanari, E. Macchi, Thermodynamic analysis of advanced power cycles based upon solid oxide fuel cells, gas turbines and Rankine bottoming cycles, ASME paper No. 98-GT-585, International Gas Turbine and Aeroengine Congress and Exhibition, Stockholm, June 1998.
[4] S.C. Singhal, Advances in solid oxide fuel cell technology, in: Proceedings of the 1998 Fuel Cell Seminar, Courtesy Associates, November 1998.
[5] M. Mozaffarian, Solid oxide fuel cell for combined heat and power applications, in: Proceedings of the First European Solid Oxide Fuel Cell Forum, Lucerne, Switzerland, 1994.
[6] J.H. Hirschenhofer, D.B. Stauffer, R.R. Engleman, Fuel Cells, A Handbook (Rev. 3), Commonwealth Inc. for US Department of Energy (DOE), Gilbert, 1994.
[7] H. Ide, et al., Natural gas reformed fuel cell power generation systems — a comparison of three system efficiencies, in: Proceedings of the 24th IECEC, Washington, 1989.
[8] N.F. Bessette, R.A. George, Electrical performance of Westinghouse's AES solid oxide fuel cell, in: Proceedings of the Second International Fuel Cell Conference, (IFCC 4–12) Japan, 1996.
[9] K. Kinoshita, F.R. McLarnon, E.J. Cairns, Fuel Cells, A Handbook, L. Berkeley Laboratory for US Department of Energy (DOE), 1988.
[10] S. Campanari, Power plants based on solid oxide fuel cells integrated with gas turbine cycles, Ph.D. Thesis, Politecnico di Milano, 1998 (in Italian).
[11] S. Veyo, The Westinghouse SOFC program — a status report, in: Proceedings of the 31st IECEC, No. 96570, 1996, pp. 1138–1143.
[12] S. Veyo, C. Forbes, Demonstrations based on Westinghouse's prototype commercial AES design, in: Proceedings of the Third European Solid Oxide Fuel Cell Forum, 1998, pp. 79–86.